ADVANCED MATERIALS
www.advmat.de

A Boron, Nitrogen, and Oxygen Doped π-Extended Helical Pure Blue Multiresonant Thermally Activated Delayed Fluorescent Emitter for Organic Light Emitting Diodes That Shows Fast k_{RISC} Without the Use of Heavy Atoms

Rangani Wathsala Weerasinghe, Subeesh Madayanad Suresh, David Hall, Tomas Matulaitis, Alexandra M. Z. Slawin, Stuart Warriner, Yi-Ting Lee, Chin-Yiu Chan, Youichi Tsuchiya,* Eli Zysman-Colman,* and Chihaya Adachi**

Narrowband emissive multiresonant thermally activated delayed fluorescence (MR-TADF) emitters are a promising solution to achieve the current industry-targeted color standard, Rec. BT.2020-2, for blue color without using optical filters, aiming for high-efficiency organic light-emitting diodes (OLEDs). However, their long triplet lifetimes, largely affected by their slow reverse intersystem crossing rates, adversely affect device stability. In this study, a helical MR-TADF emitter (*f*-DOABNA) is designed and synthesized. Owing to its π-delocalized structure, *f*-DOABNA possesses a small singlet-triplet gap, ΔE_{ST}, and displays simultaneously an exceptionally faster reverse intersystem crossing rate constant, k_{RISC}, of up to 2×10^6 s^{-1} and a very high photoluminescence quantum yield, Φ_{PL}, of over 90% in both solution and doped films. The OLED with *f*-DOABNA as the emitter achieved a narrow deep-blue emission at 445 nm (full width at half-maximum of 24 nm) associated with Commission Internationale de l'Éclairage (CIE) coordinates of (0.150, 0.041), and showed a high maximum external quantum efficiency, EQE_{max}, of ≈20%.

1. Introduction

Heteroatom-doped nanographene-based multiresonant thermally activated delayed fluorescent (MR-TADF) compounds have emerged as attractive candidates to be incorporated into commercial organic light-emitting diodes (OLEDs).[1] MR-TADF compounds are organic, brightly luminescent compounds with narrowband emission, and so, can produce the desired saturated emission required by the display application. Importantly, they can harvest both singlet and triplet excitons in OLEDs,[2,3] achieving a 100% internal quantum efficiency (IQE). Of particular relevance is the search for a high-performance blue emitter to replace the presently used triplet–triplet annihilation materials that are limited to 62.5% IQE,[1] and more importantly, do not emit with the optimal color purity.[4] Despite MR-TADF emitters possessing the desired narrowband emission and being very bright, they are relatively inefficient in promoting triplet excitons into singlet excitons owing to their generally moderately large singlet-triplet energy gap, ΔE_{ST}, the small degree of spin-orbit coupling (SOC) between these states, and too slow reverse intersystem crossing rate constants, k_{RISC}, resulting in the devices showing severe efficiency roll-off. Moreover, there are only a handful of these emitters that meet the stringent color

R. W. Weerasinghe, Y.-T. Lee, Y. Tsuchiya, C. Adachi
Center for Organic Photonics and Electronics Research (OPERA)
Kyushu University
Motooka, Nishi, Fukuoka 819-0395, Japan
E-mail: tsuchiya@opera.kyushu-u.ac.jp; adachi@opera.kyushu-u.ac.jp

S. Madayanad Suresh, D. Hall, T. Matulaitis, A. M. Z. Slawin, E. Zysman-Colman
Organic Semiconductor Centre
EaStCHEM School of Chemistry
University of St Andrews
St Andrews KY16 9ST, UK
E-mail: eli.zysman-colman@st-andrews.ac.uk

S. Warriner
School of Chemistry
University of Leeds
Woodhouse Lane
Leeds LS2 9JT, UK

The ORCID identification number(s) for the author(s) of this article can be found under https://doi.org/10.1002/adma.202402289

DOI: 10.1002/adma.202402289

requirements for displays, the most recent of which being the recommendation for broadcasting service television (Rec. BT.) 2020–2, which is defined according to the Commission International de l'Éclairage (CIE) 1931 as (0.131, 0.046) for the blue color point.[5] This is in part due to the planar core structure of most MR-TADF emitters that is prone to aggregation, leading to an undesired broadeningof the emission spectrum. To mitigate this effect, the emissive layer of the OLEDs typically only contains very low concentrations of the MR-TADF emitter.

The poor stability of devices with MR-TADF emitters is partly a consequence of their slow k_{RISC}. One strategy to improve k_{RISC} in these systems is to increase the size of the π-system, which would lead to a more delocalized short-range charge transfer (SRCT) excited state, resulting in a smaller ΔE_{ST},[6] albeit, typically at the expense of a red-shifted emission. A second benefit of having a π-extended structure is the presence of intermediate triplet states of different wavefunction characters to S_1, aiding in the acceleration of k_{RISC}.[7,8] The emitter *ν*-DABNA has a much smaller ΔE_{ST} of 17 meV,[8] a shorter delayed lifetime (τ_d) of 4.1 µs, and a faster k_{RISC} of 2.0×10^5 s^{-1} compared to those of the parent DABNA-1 (ΔE_{ST} = 196 meV, τ_d = 93.7 µs, and $k_{RISC} = 9.9 \times 10^3$ s^{-1}, **Figure 1**).[2] Hatakeyama et al. recently reported a π-extended MR-TADF emitter in the framework of a helicene (V-DABNA-Mes) that has an even smaller ΔE_{ST} of 5.2 meV, shorter τ_d of 2.39 µs, and a k_{RISC} of 4.4×10^5 s^{-1} in the 1 wt% doped films of poly(methylmethacrylate) (PMMA) when compared to the parent, *ν*-DABNA.[9] This translates to an efficient sky-blue electroluminescence (EL) in solution-processed OLEDs emitting at CIE coordinates of (0.09, 0.21) associated with a λ_{EL} of 480 nm and a maximum external quantum efficiency (EQE_{max}) of 22.9%. The same research group later modified the V-DABNA-Mes structure, replacing the peripheral mesityl units with phenyl groups.[10] This new emitter (V-DABNA) showed similar photophysical behavior to that of its parent V-DABNA-Mes, and the device showed similar performance metrics, λ_{PL} of 483 nm, full width at half-maximum (FWHM) of 17 nm, CIE coordinates of (0.09, 0.25), and EQE_{max} of 26.2%. Notably, the derivative V-DABNA-F emitted slightly bluer at 464 nm in a 1 wt% doped film in PMMA due to the presence of the electron-withdrawing 2,6-fluorophenyl units. Just like V-DABNA, V-DABNA-F maintained a very small ΔE_{ST} of 4.6 meV, a short, τ_d of 1.7 µs, and a k_{RISC} of 6.5×10^5 s^{-1} in a 1 wt% doped film in PMMA. The OLED showed an EQE_{max} of 26.6% at λ_{EL} of 468 nm and CIE coordinates of (0.12, 0.10). Although these elegant designs demonstrate that k_{RISC} can be improved to $>10^5$ s^{-1}, they also highlight how difficult it is to reach the desired blue color point. We have reported several MR-TADF compounds emitting in the deep-blue and near-UV (λ_{PL} < 450 nm); all these contain a combination of nitrogen- and oxygen-donating atoms rather than only nitrogen atoms as donors as in DABNA and related systems. In each of these examples, k_{RISC} is slow, contributing to the rather large efficiency roll-off observed in their OLEDs. For instance, NOBNacene, which emits at λ_{PL} of 410 nm (FWHM of 38 nm) in a 1.5 wt% doped film in TSPO1,[7] has a ΔE_{ST} of 0.30 eV and a k_{RISC} of 3.7×10^3 s^{-1}. The OLED with NOBNacene shows an EQE_{max} of 8.5% at λ_{EL} of 409 nm, with associated CIE coordinates of (0.173, 0.055). DIDOBNA-N emits brightly in the deep blue at λ_{PL} of 444 nm (FWHM = 64 nm) in a 1.5 wt% doped film in TSPO1 and has a ΔE_{ST} of 0.23 eV and a k_{RISC} of 3.1×10^4 s^{-1}. The deep-blue OLED shows a very high EQE_{max} of 15.3% with CIE_y of 0.073; however, a severe efficiency roll-off is observed, resulting in EQE_{100} being only 3.8%. MesB-DIDOBNA-N emits in the near-UV at λ_{PL} of 402 nm (FWHM = 19 nm) in a 1.5 wt% doped film in TSPO1 and has a ΔE_{ST} of 0.24 eV and a k_{RISC} of 9.8×10^3 s^{-1}. The OLED with MesB-DIDOBNA-N, doped in a co-host (TSPO1:CzSi = 1:1), shows the highest efficiency reported for a near-UV OLED of 16.2% with a CIE_y coordinate of 0.049 as a near-UV OLED but, unfortunately again, a severe efficiency roll-off is observed, resulting in an EQE_{100} of 3.5%.

So far, very few reports have documented OLEDs having CIE color coordinates that meet the Rec. BT. 2020-2 requirement for blue color point of 0.046 for CIE_y. One such device employed BOBO-Z as the emitter,[11] demonstrating an EQE_{max} of 13.6% at λ_{EL} of 445 nm with CIE coordinates of (0.15, 0.04). Such an outstanding device performance was in part due to the moderately small ΔE_{ST} of 102 meV and a k_{RISC} of 7.0×10^4 s^{-1} in a 3 wt% doped film with an mCBP host. We previously reported the MR-TADF emitter, 2B-DTACrs,[12] that emits at λ_{PL} of 447 nm (FWHM of 24 nm) in a 5 wt% doped film with an mCBP host. Its moderate ΔE_{ST} of 160 meV and short τ_d of 13.1 µs in a 5 wt% doped film with an mCBP host contributed to the relatively fast k_{RISC} of 1.3×10^5 s^{-1} for an MR-TADF emitter. The OLED showed an EQE_{max} of 14.8% at λ_{EL} of 447 nm, CIE coordinates of (0.150, 0.044), and an improved efficiency roll-off, with EQE_{100} of 10%. To date, blue MR-TADF OLEDs emitting at the desired CIE coordinates and showing EQE_{max} greater than 20% have seldom been reported in the literature. Thus, developing pure blue narrowband emitters that are efficient triplet harvesters is still an urgent topic for the OLED industry. Through our previous works we have demonstrated how the emission spectrum of MR-TADF emitters and OLEDs can be shifted to approach the Rec. BT.2020-2 color point for blue by modulating the number of nitrogen and oxygen donor atoms and boron acceptor atoms within the π-extended framework.[7,12,13] However, these prior examples also revealed that each of these emitters possessed reasonably large ΔE_{ST} compared to the reported B,N-doped DABNA type π-extended systems, which have ΔE_{ST} values that are often much smaller.[8,10] A small ΔE_{ST} value alone does not guarantee a fast k_{RISC}. Another feature of π-extended MR-TADF systems is the relatively large SOC between low-lying triplet states and S_1, which in some cases, may be mediated by the presence of triplet states (T_n) of intermediate energy between T_1 and S_1 that possess different orbital types to the latter; while in other cases, S_1 and T_1 have sufficiently different orbital types to produce the large SOC between the two. Only when these two design precepts work in tandem, k_{RISC} will become fast in MR-TADF emitters.

Building upon our previous studies,[7,12,13] in this work, we designed a hybrid structure of DABNA and DOBNA fragments that

C.-Y. Chan
Department of Materials Science and Engineering
City University of Hong Kong
Tat Chee Avenue, Kowloon, Hong Kong 000-000, China
E-mail: chinychan2@cityu.edu.hk
C.-Y. Chan
Department of Chemistry
City University of Hong Kong
Tat Chee Avenue, Kowloon, Hong Kong 000-000, China

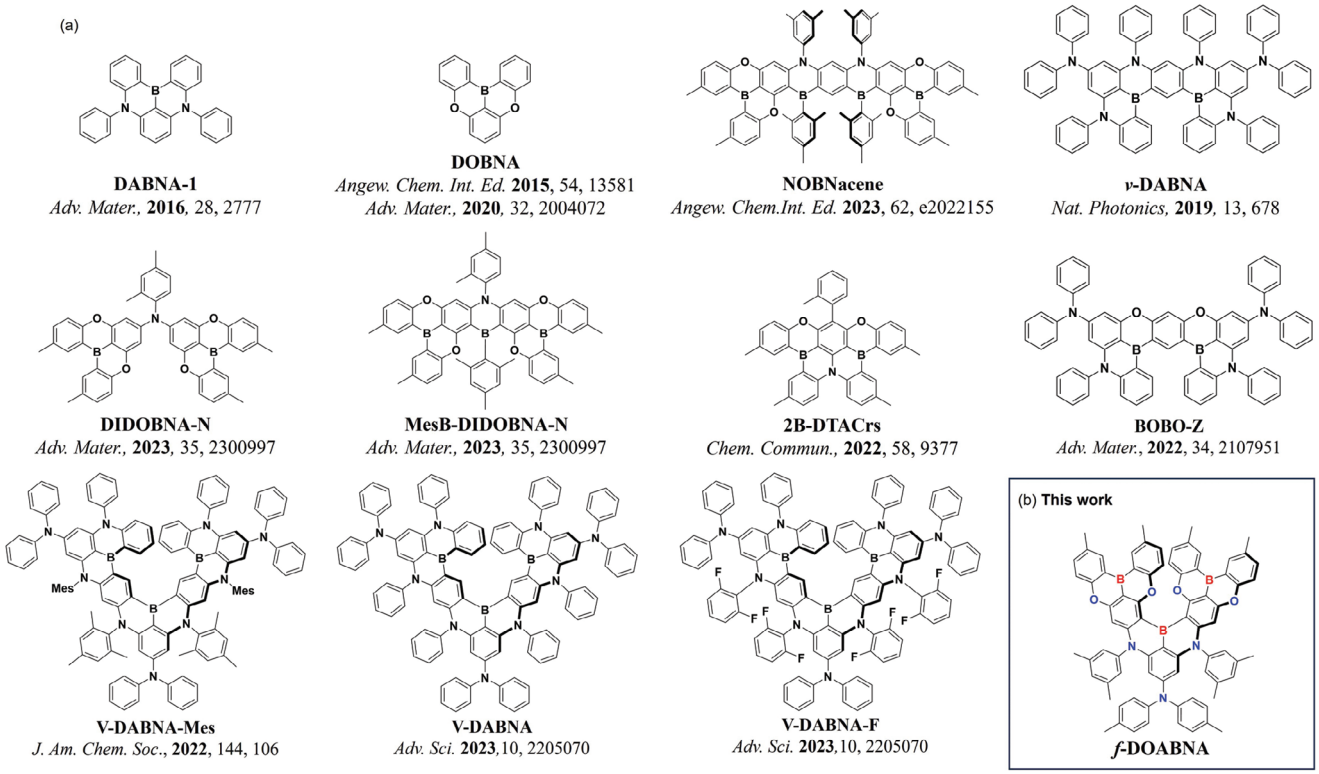

Figure 1. a) Chemical structures of blue MR-TADF compounds and b) *f*-DOABNA.

would simultaneously possess a small ΔE_{ST} and large SOC that would accelerate k_{RISC}. In contrast to enhancing the SOC of an MR-TADF emitter with the help of heavy atoms, which often increase ISC and provoke the extension of exciton lifetime, we proposed an alternative strategy to enhance SOC; while, avoiding the use of chemically unstable carbon-heavy atom bonds, thereby improving the stability and reliability of the material[14] The boron-, nitrogen- and oxygen-doped.[8]-helicene MR-TADF material (*f*-DOABNA) has, to the best of our knowledge, a record fast k_{RISC} for a blue MR-TADF emitter with a $\lambda_{PL} < 450$ nm (Figure 1).[8,10] In toluene solution, *f*-DOABNA emits at λ_{PL} of 445 nm (FWHM of 18 nm), has a very small ΔE_{ST} of 20 meV, a short τ_d of 2.12 µs, and a very high k_{RISC} of 1.0×10^6 s^{-1} for a MR-TADF emitter. The OLED with *f*-DOABNA showed an EQE_{max} of 19.5%, and critically, emitted at λ_{EL} of 445 nm (FWHM of 24 nm) at CIE coordinates of (0.150, 0.041) that were very close to the Rec. BT. 2020-2 requirement for the blue pixel of (0.131, 0.046).

2. Results and Discussion

The synthetic scheme for *f*-DOABNA is outlined in **Figure 2** and was synthesized in a four-step reaction sequence. Similar in synthetic methodology to that previously employed by us,[7] we first installed DOBNA fragments before initiating a final borylation reaction to afford *f*-DOABNA. This two-stage borylation strategy helped to precisely control the borylation sites in π-extended structures without the need for installation of directing groups. Compound 1 was obtained in an 81% yield from 3,5-dichlorobromobenzene following a Buchwald–Hartwig cross-coupling reaction (Figures S1–S3, Supporting Information). The compound 2 was obtained by coupling two equivalents of 3,5-dimethylaniline with 1 under Buchwald–Hartwig conditions in an 80% yield (Figures S4–S6, Supporting Information). The key intermediate, compound 3, was obtained in 60% yield by coupling two equivalents of DOBNA-Br with 2 (Figures S7–S9, Supporting Information). Electrophilic borylation of 3 with BBr_3 proceeded in 40% yield to afford the target blue emitter, *f*-DOABNA. The structure and purity of *f*-DOABNA were confirmed by ^1H and ^{13}C NMR spectroscopy, high-resolution mass spectrometry (HRMS), single crystal X-ray diffraction (SCXRD) analysis, high-performance liquid chromatography-gel permeation chromatography (HPLC-GPC), and elemental analysis (EA) (Figures S10–S14, Supporting Information).

Single crystals of *f*-DOABNA (CCDC: 2331352) were obtained by slow diffusion of hexane vapors onto the saturated solution of *f*-DOABNA in THF over several days. The crystal structures are given in Figure 2b. There are no specific interactions but the helically twisted structure of *f*-DOABNA is confirmed. The centroid-to-centroid distance between the overlapping phenyl rings of DOBNA fragments is 3.592 Å. The corresponding distance between the outer phenyl rings of the DOBNA fragment is measured to be 12.305 Å. These distances are comparable to the DABNA-type helicene structure, V-DABNA-Mes, reported previously.[9] Thermal gravimetric analysis (TGA) carried out on *f*-DOABNA under a nitrogen atmosphere reveals the decomposition temperature to be 562 °C, suggesting its high thermal stability (Figure S15, Supporting Information).

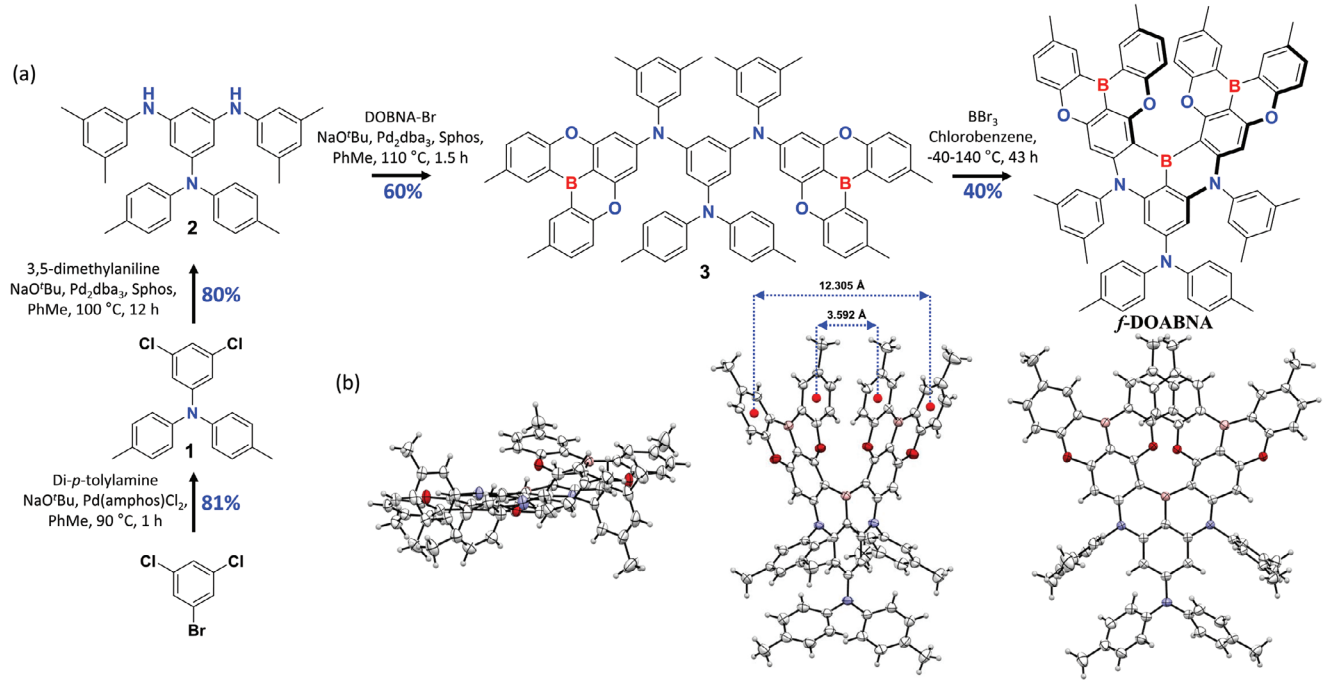

Figure 2. a) Synthesis of *f*-DOABNA. b) ORTEP images providing different orientations for single crystal structure of *f*-DOABNA. Only one enantiomer of the racemate is shown in the Figure. Single crystal analysis reveals that the crystal exists as a racemic mixture of *f*-DOABNA. Thermal ellipsoids are displayed at 50% probability.

The ground-state optimizations are carried out using density functional theory (DFT) at the PBE0/6-31G(d,p) level in the gas phase (Figure S17, Supporting Information). The excited-state optimizations of the S_1 and T_1 states are carried out using the time-dependent density functional theory within the Tamm–Dancoff approximation (TDA-DFT) with the same functional and the basis set in the gas phase. Excited-state energies are modeled using the spin-component scaling second-order approximate coupled-cluster (SCS-CC2) method using cc-pVDZ basis set, based on both the ground and excited S_1 and T_1 state geometries, calculated using DFT and TDA-DFT, respectively (**Figures 3**; and S18, Supporting Information) at the PBE0/6-31G(d,p) level. This method of calculation has proven to be successful in accurately predicting the excited-state properties of MR-TADF systems previously.[6,15,16] At the DFT level, the HOMO was mainly localized on the weak donor diphenylamine (DPA) unit and the phenylene connected to the DPA unit; whereas, the LUMO was mainly localized on the DOBNA cores. The calculated HOMO and LUMO were −5.44 and −1.40 eV, respectively, which were comparable to our previously reported emitters DIDOBNA and MesDIDOBNA (HOMOs: −5.49 and −5.56 eV and LUMOs: −1.51 and −1.46 eV, respectively).[13] The S_1 and T_1 energies calculated at the SCS-CC2 level based on the respective relaxed geometries were 3.21 and 3.18 eV, leading to a very small ΔE_{ST} of 0.03 eV that was comparable in magnitude to that of *ν*-DABNA (discussion and data of the reported vertically excited calculations are found in the Supporting Information).[16] Further, calculations predicted a closely lying T_2 state with non-negligible SOC to S_1 (0.01 cm^{-1}), which would contribute to the relatively fast reported k_{RISC}. The difference density plot for the S_1 excited state showed an alternating pattern of increasing and decreasing electron density, reminiscent of MR-TADF emitters, highlighting that this state had an SRCT character. Importantly, the nature of the excited state of T_1 was distinct from that of S_1, being reminiscent of an LE excited state, with density delocalized onto the DPA unit. Thus, the SOC constant between T_1 and S_1 of 0.44 cm^{-1} was much larger than that of most MR-TADF compounds, contributing to a much faster k_{RISC}.

The photophysical properties of *f*-DOABNA in toluene solution (1.0×10^{-5} mol L^{-1}) are shown in **Figure 4a,b**, and the data are summarized in **Table 1**. The absorption spectrum of *f*-DOABNA has a strong absorption band ($\epsilon = 9.58 \times 10^4$ L mol^{-1} cm^{-1}) at 369 nm and a weak band ($\epsilon = 2.49 \times 10^4$ L mol^{-1} cm^{-1}) at 428 nm, which are assigned to π–π^* and SRCT transitions, respectively. According to SCS-CC2 calculations, the higher intensity, higher energy band at 369 nm is assigned to a singlet state beyond the calculated S_2 state. The calculated S_1 and S_2 states have comparable oscillator strengths of 0.12 and 0.13, respectively; therefore, these states are not associated with the high-intensity band. We do not calculate higher-lying singlet states owing to the significant computational cost. The intensity of the SRCT band is comparable to those of V-DABNA-Mes, V-DABNA, and V-DABNA-F (ϵ ranging from 3.7 to 4.8 $\times 10^4$ L mol^{-1} cm^{-1}).[10] *f*-DOABNA emits at 442 nm in toluene with a very narrow FWHM of 18 nm. The emission spectrum at 77 K contains two contributions, one at 442 nm originating from prompt fluorescence and the other at 457 nm assigned to phosphorescence (Figure S19, Supporting Information). The ΔE_{ST} values for *f*-DOABNA in toluene are determined using total emission and phosphorescence spectra at 77 K after applying the Jacobian conversion (Figure S20 and Table S2, Supporting Information). From the onset values, the S_1 and T_1 energies are estimated to be 2.89

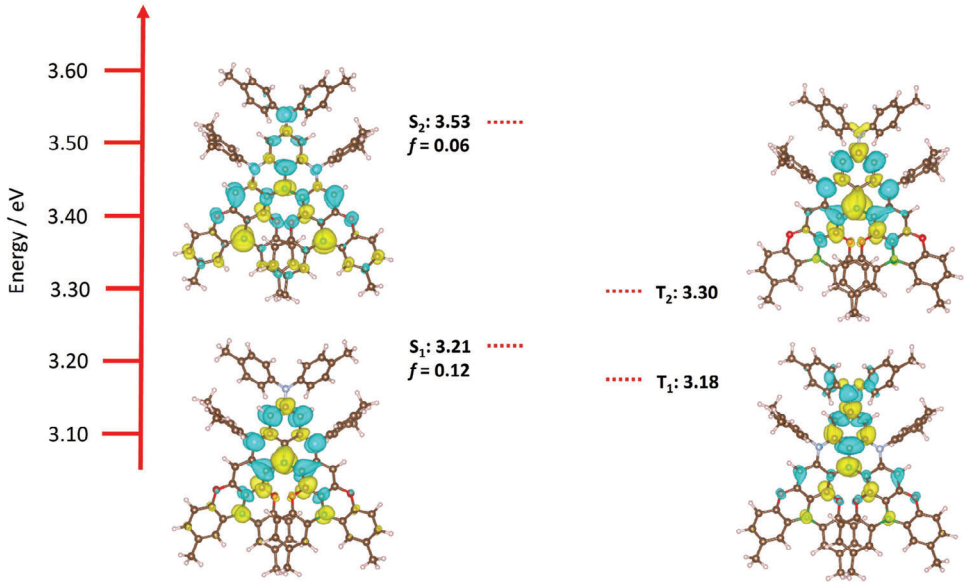

Figure 3. Excited-state energies and difference density plots of S_1, S_2, T_1, and T_2 calculated at SCS-CC2/cc-pVDZ based on the respective S_1 and T_1 optimized excited-state geometries calculated at TDA-PBE0/6-31G(d,p), (isovalue = 0.001) of *f*-DOABNA. *f* denotes the oscillator strength for the transition to the excited singlet state.

and 2.81 eV, respectively, resulting in a ΔE_{ST} of 0.08 eV. Moreover, the resulting ΔE_{ST} from the difference between the peak maxima of the fluorescence and phosphorescence spectra is determined to be 0.10 eV. This is slightly larger than the predicted ΔE_{ST} from SCS-CC2/cc-pVDZ calculations of 0.03 eV. *f*-DOABNA has an absolute photoluminescence quantum yield (Φ_{PL}) of 46% in aerated toluene solution, which increases to Φ_{PL} of 93% in an Ar-saturated toluene solution, implicating a significant contribution of triplets to the light emission process. Further, such a high Φ_{PL} is evidence of negligible nonradiative decay even in the solution media where molecular vibrations and solute-solvent interactions typically contribute to enhanced nonradiative rates.

The transient decay profile of *f*-DOABNA in Ar saturated toluene solution (Figure 4b) shows prompt and delayed emission components, with lifetimes, τ_p and τ_d, of 3.34 ns and 1.93 µs, respectively. The PL decay under aerated conditions only shows prompt emission, with τ_p of 2.99 ns. The rate constants of radiative and non-radiative decay from the singlet state k_r, k_{nr}, intersystem crossing (k_{ISC}), and k_{RISC} are calculated according to our previously developed methodology (Table 1).[17] The possible range of rate constants related to the non-radiative pathways is summarized in Table S3, Supporting Information. The large k_r (1.05×10^8 s^{-1}) and relatively small k_{nr} (7.92×10^6 s^{-1}) explain the high Φ_{PL} of *f*-DOABNA in toluene. Remarkably, *f*-DOABNA has a very fast k_{RISC} of 1.01×10^6 s^{-1}, which is one of the highest values amongst reported MR-TADF molecules, particularly those without the incorporation of heavy atoms.[3,18] The exceptionally fast k_{RISC} of *f*-DOABNA is ascribed to a combination of

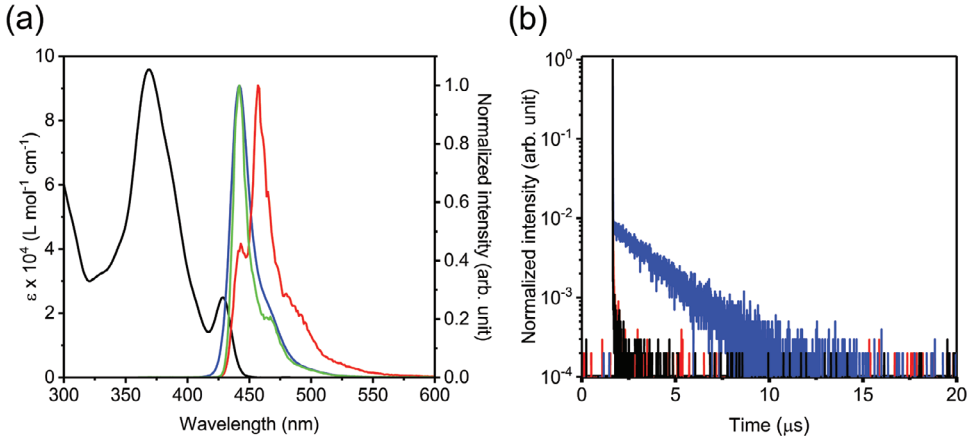

Figure 4. a) Absorption (black line), steady-state PL at RT (blue line, λ_{exc} = 340 nm), steady-state PL at 77 K (green line), and phosphorescence spectra at 77 K (red line, delay 270 ms, gate 20 ms) of *f*-DOABNA in toluene (1.0×10^{-5} mol L^{-1}). b) Time-resolved emission decays at 300 K (λ_{exc} = 340 nm) under Ar saturated (blue line), aerated conditions (red line), and IRF (black line).

Table 1. Solution-state and film-state photophysical properties of 1wt% *f*-DOABNA doped films.

	Φ_{PL} [a] [%]	λ_{PL} [b] [nm]	FWHM [nm]	ΔE_{ST} [c] [eV]	τ_p [d] [ns]	τ_d [d] [μs]	Φ_{PF}/Φ_{DF} [%]	k_r [e] (10^8 s^{-1})	k_{ISC} [e] (10^8 s^{-1})	k_{RISC} [e] (10^6 s^{-1})	k_{nr} [e] (10^7 s^{-1})
Toluene	93	442	18	0.08	3.34	1.93	44/49	1.05	1.08	1.02	0.79
DOBNA-Tol	90	444	25	0.06	6.20	0.50	75/14	1.21	0.28	2.30	1.50
*m*CP	80	447	24	0.07	3.67	1.22	46/34	1.11	1.13	1.41	3.28
DPEPO	69	450	32	0.09	3.04	1.47	45/24	1.51	1.09	1.02	6.77

[a] Absolute Φ_{PL} of thin films measured using an integrating sphere under Ar saturated condition; [b] Fluorescence maximum at RT. λ_{exc} = 340 nm in toluene and λ_{exc} = 310 nm for doped films; [c] S_1 and T_1 energies determined from the onset of the total emission and phosphorescence spectra at 77 K, respectively; [d] Prompt and delayed lifetimes obtained under Ar-saturated conditions; [e] Rate constants were calculated using three-state model approximating no phosphorescence in emission.

its very small ΔE_{ST} and the distinct character of each of the S_1 and T_1 states that contribute to the significant SOC between these two states (0.44cm^{-1}), unlike what exists in most MR-TADF compounds where S_1 and T_1 possess the same orbital types.[16] The presence of a weak positive solvatochromatic effect (13.7 nm) on the emission wavelength of *f*-DOABNA upon changing the solvent polarity from non-polar toluene to polar acetonitrile is strong evidence for the SRCT character of the emissive excited state of *f*-DOABNA (Figure S21 and Table S4, Supporting Information). However, it is a slightly larger value than other reported boron-containing MR-TADF emitters.[3]

We next investigated the thin film photophysics of *f*-DOABNA in a 1 wt% doped in three different host materials: bis[2-(diphenylphosphino)phenyl]ether oxide (DPEPO), 1,3-bis(*N*-carbazolyl)benzene (*m*CP), and 3,11-di-*o*-tolyl-5,9-dioxa-13b-boranaphtho[3,2,1-de]anthracene (DOBNA-Tol) (**Figure 5**). These three hosts were chosen as they each have very high T_1 levels of 3.00, 2.97, and 2.91 eV for DPEPO, DOBNA-Tol, and *m*CP, respectively. The 1 wt% *f*-DOABNA doped films in all three hosts showed high Φ_{PL} values, ranging from 69% to 90%. However, even at this low doping concentration, all films showed slightly red-shifted and broader emission spectra than those in toluene (Table 1). The most pronounced 9 nm red-shift (FWHM of 32 nm) occurred in a DPEPO film, which had the largest dipole moment of 5.5 D compared with *m*CP (1.35 D) and DOBNA-Tol (1.51 D).[19] The lower doping level (0.5 wt%) of *f*-DOABNA in DPEPO exhibited narrower emission (FWHM of 30 nm), and the FWHM increased with increasing doping concentration, indicating the presence of molecular aggregation even at 1 wt% doping levels. However, a drop in the Φ_{PL} to 48% was observed in the 0.5 wt% *f*-DOABNA:DPEPO film due to the incomplete energy transfer that was evidenced by the presence of host emission (Figure S22 and Table S5, Supporting Information). The PL of the 0.5 wt% *f*-DOABNA: *m*CP film matched that of 1 wt% doped film (Figure S22 and Table S5, Supporting Information); while, that of the 2 wt% doped film showed a shoulder at ≈500 nm, which we could attribute to aggregate emission. The most favorable emission behavior of *f*-DOABNA was observed in DOBNA-Tol as the bluest PL at 444 nm and the highest Φ_{PL} of 90% were registered in the 1 wt% doped film. The delayed lifetime showed a remarkably short τ_d of 0.5 μs compared to that of other reported MR-TADF materials.[3] The exceptionally short delayed lifetime translated to a very high k_{RISC} value of 2.3×10^6 s^{-1} for *f*-DOABNA in DOBNA-Tol. In accordance with their k_{RISC} values, the τ_d of *f*-DOABNA in *m*CP and DPEPO were somewhat longer at 1.22 and 1.47 μs, respectively; yet, nonetheless remained very short compared to those of other MR-TADF emitters.

In addition, the temperature dependence of the transient emission decay profiles of 1 wt% *f*-DOABNA in the most promising host materials, *m*CP and DOBNA-Tol, was measured (Figure S22, Supporting Information). In both films, the intensity of the delayed emission component increased upon increasing the temperature from 150 to 300 K, in line with typical TADF behavior (Figure S23a,b, Supporting Information). Further, the temperature dependency on k_{ISC} and k_{RISC} for both films was analyzed using an Arrhenius plot to determine the activation energy (E_a) for both processes (Figure S24a–d, Supporting Information). Thereby, the ΔE_{ST} values for both films were calculated from the difference in the activation energies between the k_{ISC} and k_{RISC}

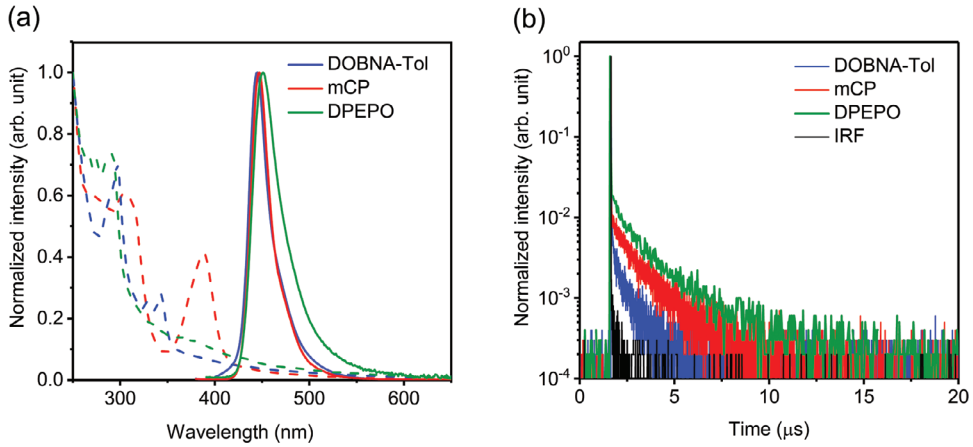

Figure 5. Photophysical properties of 1 wt% of *f*-DOABNA doped in different hosts: a) Normalized absorption (dotted lines), and fluorescence (solid lines, λ_{exc} = 310 nm) spectra. b) Transient decay curves (λ_{exc} = 280 nm) under the degassed conditions for hosts DOBNA-Tol, *m*CP and DPEPO, and the IRF (black line) at 300 K.

processes. For the 1wt% *f*-DOABNA in *m*CP and DOBNA-Tol hosts, the calculated ΔE_{ST} values were 30.9 and 19.6 meV, respectively. The smaller ΔE_{ST} of *f*-DOABNA in DOBNA-Tol explains the faster k_{RISC} of this film compared to that of *f*-DOABNA in the *m*CP host.

Recognizing the outstanding photophysical properties of *f*-DOABNA, we fabricated OLEDs using the following structure considering the energy level alignment of the materials (**Figures** 6a; and S25, Supporting Information): indium-tin-oxide (ITO)-coated glass/TAPC (55 nm)/*m*CP (15 nm)/1 wt% *f*-DOABNA in DOBNA-Tol or *m*CP (30 nm)/PPT (10 nm)/BPy-TP2 (30 nm)/Liq (2 nm)/Al (100 nm), where, TAPC, *m*CP, *f*-DOABNA in DOBNA-Tol, PPT, BPy-TP2, and Liq were the hole-transporting, electron-blocking, emitting, hole-blocking,

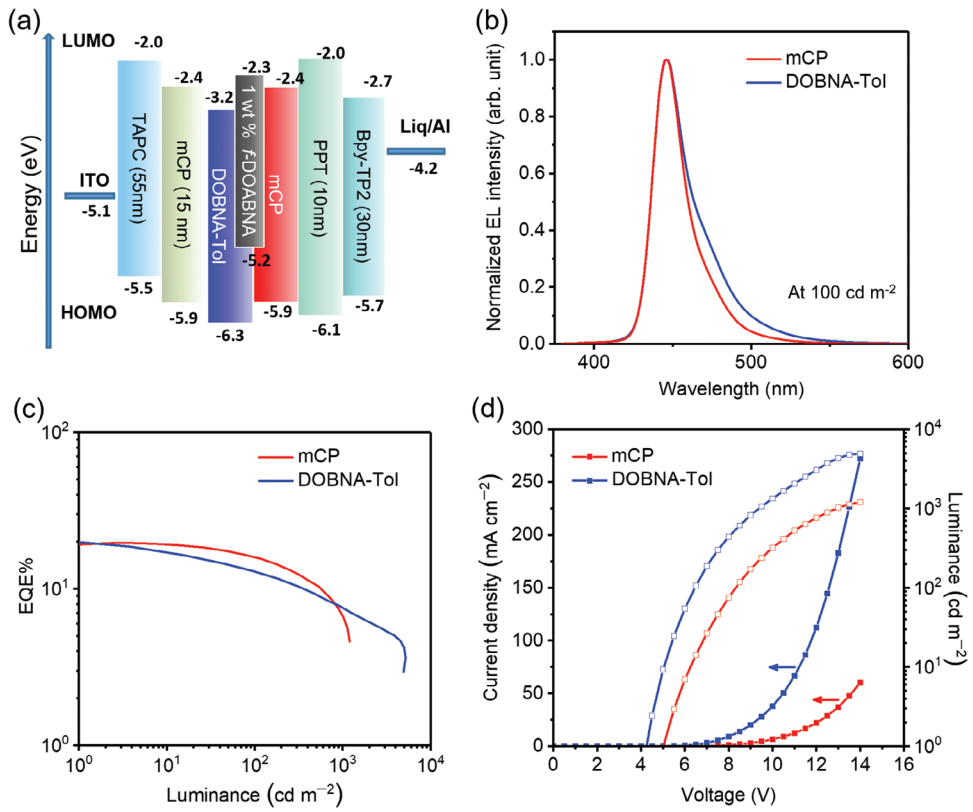

Figure 6. OLED performance of *f*-DOABNA (1 wt%) doped in *m*CP (red line) and DOBNA-Tol (blue line) hosts: a) device structure, b) electroluminescence spectra at 100 cd m^{-2}, c) EQE versus luminance curves, and d) current density (closed circle) and luminance (open circle) versus driving voltage curves.

Table 2. Device performance of *f*-DOABNA in DOBNA-Tol or *m*CP as a host in emissive layer.

Host	V_{on} [V]	EQE_{max} [%]	$EQE_{100/1000}$ [%]	Lum_{max} [cd m^{-2}]	CE [cd A^{-1}]	PE [lm W^{-1}]	λ_{EL} [nm]	FWHM [nm]	CIE
DOBNA-Tol	4.2	19.9	12.9/6.7	4858	11.4	8.4	445	28	0.153, 0.056
*m*CP	5.0	19.5	15.9/7.5	1194	7.6	4.7	445	24	0.150, 0.041

electron-transporting, and electron injection layers, respectively. The device data are presented in **Table 2**. Both DOBNA-Tol-based and *m*CP-based devices showed EQE_{max} values of nearly 20% coupled with narrowband blue emissions (Figure 6b,c). The high EQE_{max} values of both devices could be attributed to the high Φ_{PL} and k_{RISC} value of *f*-DOABNA; however, the DOBNA-Tol-based device displayed a lower turn-on voltage of 4.2 V compared to that of the *m*CP-based device of 5.0 V (Figure 6d). The lower driving voltage was based on a smaller energy barrier for electron injection due to the lower LUMO of DOBNA-Tol compared to that of *m*CP. Both DOBNA-Tol and *m*CP-based devices emitted at λ_{EL} of 445 nm, which aligned closely with the PL spectra of *f*-DOABNA. The EL of the *m*CP-based device showed the desired blue emission, with a CIE_y of 0.041, which satisfied the Rec. BT.2020-2. This was due to the deep blue emission with a narrow FWHM of 24 nm. To the best of our knowledge, *f*-DOABNA-based devices are the best MR-TADF OLEDs reported in the literature, considering the simultaneous achievement of narrowband emission (FWHM < 30 nm) and high EQEmax (nearly 20%); while, satisfying Rec. BT. 2020–2 for blue pixels (Figures S26 and S27, Supporting Information).

To rationalize the origin of the high efficiency, we conducted angle-dependent PL measurements on the 1 wt% *f*-DOABNA doped films in *m*CP and DOBNA-Tol hosts to assess whether the transition dipole moments (TDM) of the emitter were preferentially oriented in these hosts, which would contribute to enhanced light-outcoupling efficiency (**Figure 7**). The TDM orientation of *f*-DOABNA in the films was analyzed with SETFOS where the horizontal-dipole ratios (Θ) of 0, 0.33, and 1 corresponded to perfectly horizontal, isotropic, and vertical orientation, respectively. The *f*-DOABNA doped film in an *m*CP host provided Θ = 0.21, meaning 79% horizontal alignment of the TDM. The TMD horizontal orientation of *f*-DOABNA doped in DOBNA-Tol was slightly weaker, resulting in Θ = 0.26. Thus, the simulated light outcoupling efficiency with these devices using SETFOS was 26% and 24% using *m*CP and DOBNA-Tol hosts, respectively, indicating a rather small difference in the outcoupling efficiencies. Despite the faster k_{RISC} of *f*-DOABNA in DOBNA-Tol, the unfavorable roll-off at the low current density region observed in DOBNA-Tol based devices could be attributed to the disparities in carrier transporting properties between the host materials, where *m*CP and DOBNA-Tol showed the bipolar and n-type host properties, respectively (Figure S28, Supporting Information). Owing to the unbalanced carrier transporting property of DOBNA-Tol, the charge recombination zone of DOBNA-Tol-based device should be near the interface of *m*CP in the emissive layer. Considering the HOMO energy levels of DOBNA-Tol and *m*CP, direct exciton formation would happen on *f*-DOBNA at the low current density. Therefore, increase of the current density produces significant polaron (electron)–exciton annihilation in DOBNA-Tol-based devices because of the further electron accumulation at the interface.

3. Conclusion

In summary, a deep-blue helical MR-TADF emitter, *f*-DOABNA, had been successfully designed and synthesized. *f*-DOABNA exhibited a small ΔE_{ST} of 80 meV, and the π−delocalized structure resulted in a high SOC of 0.44 cm^{-1}, which led to a short delayed lifetime of 1.93 µs and an extraordinarily fast k_{RISC} rate of 1.02×10^6 s^{-1} in toluene. Most importantly, *f*-DOABNA emitted a

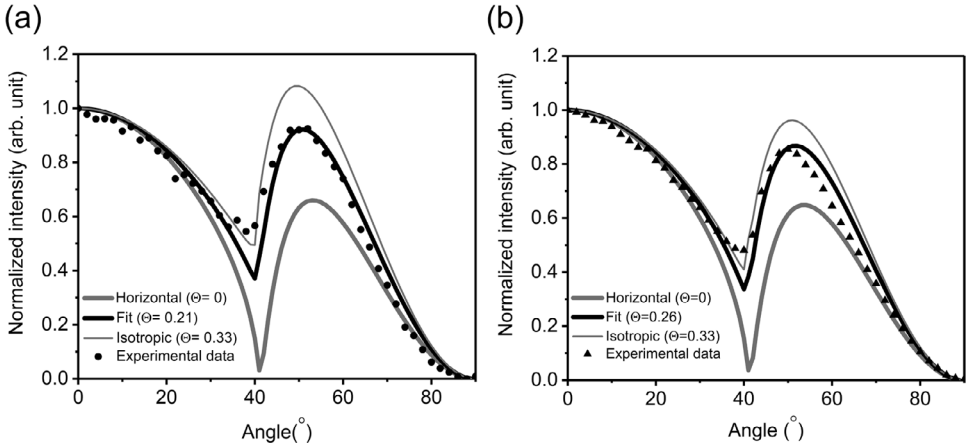

Figure 7. Angular-dependent PL profiles of 1 wt% *f*-DOABNA doped in *m*CP (a, closed circle) and DOBNA-Tol (b, closed triangle). The horizontal (thick gray line), isotropic (thin gray line), and fitting curves for the experimental data (black line) were provided using the optical simulation software SETFOS 4.6 (Fluxim).

deep-blue color at 442 nm with a narrow FWHM of 18 nm and a high Φ_{PL} of 0.93. When doping 1 wt% of *f*-DOABNA in DOBNA-Tol and *m*CP hosts, both doped films displayed slightly broadened emissions compared to that observed in toluene. Despite wider FWHMs, the k_{RISC} was further enhanced up to 2.3×10^6 s^{-1} in 1 wt% doped film in DOBNA-Tol, which, to our best knowledge, represents one of the best values in k_{RISC} for deep-blue MR-TADF emitters. Devices based on the *m*CP host showed a high EQE_{max} of 20% and achieved CIEs of (0.150, 0.041), which is the very first time for deep-blue MR-TADF emitter achieving CIEy = 0.04 with a high EQE_{max} of 20% and a narrow FWHM of only 24 nm. These results suggest that the MR-TADF emitter with a delocalized π-structure is a promising candidate for the application in commercial UHD displays.

Supporting Information

Supporting Information is available from the Wiley Online Library or from the author.

Acknowledgements

R.W.W. and S.M.S contributed equally to this work. The authors acknowledge Ms. N. Nakamura and Ms. K. Kusuhara for their technical assistance with this research. This work was supported financially by the JSPS Core-to-Core Program (grant number: JPJSCCA20180005), JSPS International Leading Research (ILR) (Grant No. 23K20039), JSPS Grant-in-Aid for Specially Promoted Research (Grant No. 23H05406), Kyulux Inc, and the Engineering and Physical Sciences Research Council for support (EP/R035164/1; EP/W007517/1). C.-Y.C acknowledges the support from the grant from the City University of Hong Kong (Project Nos. 9610637 and 9231531). This project has received funding from the European Union's Horizon 2020 research and innovation programme under the Marie Skłodowska-Curie grant agreement No 838885 (NarrowbandSSL). S.M.S. acknowledges support from the Marie Skłodowska-Curie Individual Fellowship (grant agreement No. 838885 NarrowbandSSL). Computational resources have been provided by the Consortium des Équipements de Calcul Intensif (CÉCI), funded by the Fonds de la Recherche Scientifiques de Belgique (F. R. S.-FNRS) under Grant No. 2.5020.11, as well as the Tier-1 supercomputer of the Fédération Wallonie-Bruxelles, infrastructure funded by the Walloon Region under the grant agreement n1117545.

Conflict of Interest

The authors declare no conflict of interest.

Data Availability Statement

The research data supporting this publication can be accessed at https://doi.org/10.17630/75e623ff-0a7d-4ede-ba97-bf5622a5f9db.

Keywords

blue emitter, boron, multiresonant thermally activated delayed fluorescence, organic light-emitting diodes, reverse intersystem crossing

Received: February 13, 2024
Revised: April 3, 2024
Published online: April 18, 2024

[1] H. J. Kim, T. Yasuda, *Adv. Opt. Mater.* **2022**, *10*, 2270086.
[2] T. Hatakeyama, K. Shiren, K. Nakajima, S. Nomura, S. Nakatsuka, K. Kinoshita, J. Ni, Y. Ono, T. Ikuta, *Adv. Mater.* **2016**, *28*, 2777.
[3] S. M. Suresh, D. Hall, D. Beljonne, Y. Olivier, E. Zysman-Colman, *Adv. Funct. Mater.* **2020**, *30*, 1908677.
[4] H. Jiang, P. Tao, W. Y. Wong, *ACS Mater. Lett.* **2023**, *5*, 822.
[5] In *BT.2020-2 (10/2015)*, International Telecommunication Union, Geneva, Switzerland **2015**, Vol. *2015-10*
[6] A. Pershin, D. Hall, V. Lemaur, J. C. Sancho-Garcia, L. Muccioli, E. Zysman-Colman, D. Beljonne, Y. Olivier, *Nat. Commun.* **2019**, *10*, 597.
[7] S. M. Suresh, L. Zhang, D. Hall, C. Si, G. Ricci, T. Matulaitis, A. M. Z. Slawin, S. Warriner, Y. Olivier, I. D. W. Samuel, E. Zysman-Colman, *Angew. Chem., Int. Ed.* **2023**, *62*, 202215522.
[8] Y. Kondo, K. Yoshiura, S. Kitera, H. Nishi, S. Oda, H. Gotoh, Y. Sasada, M. Yanai, T. Hatakeyama, *Nat. Photonics* **2019**, *13*, 678.
[9] S. Oda, B. Kawakami, Y. Yamasaki, R. Matsumoto, M. Yoshioka, D. Fukushima, S. Nakatsuka, T. Hatakeyama, *J. Am. Chem. Soc.* **2022**, *144*, 106.
[10] S. Oda, B. Kawakami, M. Horiuchi, Y. Yamasaki, R. Kawasumi, T. Hatakeyama, *Adv. Sci.* **2023**, *10*, 2205070.
[11] I. S. Park, M. Yang, H. Shibata, N. Amanokura, T. Yasuda, *Adv. Mater.* **2022**, *34*, 2107951.
[12] C.-Y. Chan, S. M. Suresh, Y.-T. Lee, Y. Tsuchiya, T. Matulaitis, D. Hall, A. M. Z. Slawin, S. Warriner, D. Beljonne, Y. Olivier, C. Adachi, E. Zysman-Colman, *Chem. Commun.* **2022**, *58*, 9377.
[13] S. M. Suresh, L. Zhang, T. Matulaitis, D. Hall, C. Si, G. Ricci, A. M. Z. Slawin, S. Warriner, D. Beljonne, Y. Olivier, I. D. W. Samuel, E. Zysman-Colman, *Adv. Mater.* **2023**, *35*, 2300997.
[14] N. Lin, J. Qiao, L. Duan, L. Wang, Y. Qiu, *J. Phys. Chem. C* **2014**, *118*, 7569.
[15] D. Hall, K. Stavrou, E. Duda, A. Danos, S. Bagnich, S. Warriner, A. M. Z. Slawin, D. Beljonne, A. Köhler, A. Monkman, Y. Olivier, E. Zysman-Colman, *Mater. Horiz.* **2022**, *9*, 1068.
[16] D. Hall, J. C. Sancho-García, A. Pershin, G. Ricci, D. Beljonne, E. Zysman-Colman, Y. Olivier, *J. Chem. Theory Comput.* **2022**, *18*, 4903.
[17] Y. Tsuchiya, S. Diesing, F. Bencheikh, Y. Wada, P. L. dos Santos, H. Kaji, E. Zysman-Colman, I. D. W. Samuel, C. Adachi, *J. Phys. Chem. A* **2021**, *125*, 8074.
[18] J.-M. Teng, Y.-F. Wang, C.-F. Chen, *J. Mater. Chem. C* **2020**, *8*, 11340.
[19] a) B. A. Naqvi, M. Schmid, E. Crovini, P. Sahay, T. Naujoks, F. Rodella, Z. Zhang, P. Strohriegl, S. Bräse, E. Zysman-Colman, W. Brütting, *Front. Chem.* **2020**, *8*, 33102430; b) The dipole moment of DOBNA-Tol was calculated at its most stable ground-state conformation at the B3LYP/6-31G** level of theory because of its structural rigidity.